Electronic Supplementary Material (ESI) for Materials Horizons.

Ferroelectrically tunable magnetic skyrmions in two-dimensional multiferroics

Zhonglin He, Wenhui Du, Kaiying Dou, Ying Dai*, Baibiao Huang, Yandong Ma*

School of Physics, State Key Laboratory of Crystal Materials, Shandong University, Shandanan Street 27, Jinan 250100, China

*Corresponding author: daiy60@sina.com (Y.D.); yandong.ma@sdu.edu.cn (Y.M.)

Supplementary Note 1: Computational details of first-principles calculations and MC simulations

Our first-principles calculations are performed on the basis of the density-functional theory (DFT), as implemented in the Vienna Ab initio Simulation Package (VASP) [1-3]. Considering the exchange-correlation interaction, the generalized gradient approximation (GGA) in the form of Perdew-Burke-Ernzerhof functional is utilized [4]. The cutoff energy is set to 500 eV, and the convergence criterion of total energy is set to 10^{-5} eV. Structures are fully relaxed until the force on each atom is less than 10^{-2} eV/Å, and a 15 × 15 × 1 *k*-point mesh is used to sample the Brillouin zone. For magnetic parameters calculations, a 2×1 supercell with a k-point mesh of 16 × 32 × 1 is used, while in DMI calculations, a 4×1 supercell with a k-point mesh of 8 × 32 × 1 is used. To avoid interaction between adjacent layers, a vacuum space of 30 Å is adopted. To describe the strong correlated correction of Co-3d electrons, the GGA+U method is employed [5], and the U value is chosen as 2 eV.

Using the magnetic parameters obtained from first-principles calculations, parallel tempering Monte-Carlo (MC) simulations with the Metropolis algorithm are carried out to get the energy minimum spin textures [9]. The spin textures are obtained based on a 210 × 210 × 1 supercell with 1 × 10^5 MC steps performed for each temperature (from 660 K gradually cooling down to 0 K).

meV	J	K_C	λ	K_S	$d_{\parallel}$	κ	κ'
Co_2NF_2	3.61	0.81	-0.04	-0.16	-1.01	2.3	1.8
$Co_2NF_2/MoSe_2$ (FE1)	3.24	-0.16	0.09	-0.15	-1.06	-1.0	-0.2
$Co_2NF_2/MoSe_2$ (FE2)	2.77	0.34	0.05	-0.15	0.96	0.6	1.0

Table. S1. Magnetic parameters of Co_2NF_2 and $Co_2NF_2/MoSe_2$.

Supplementary Note 2: The formulas of $\{^{1}e_x, {}^{1}e_y\}$ and $\{^{2}e_x, {}^{2}e_y\}$.

$$1e_x = \sqrt{2/3}d_{xy} - \sqrt{1/3}d_{xz},$$
$$1e_y = \sqrt{2/3}d_{x^2-y^2} - \sqrt{1/3}d_{yz},$$
$$2e_x = \sqrt{1/3}d_{xy} + \sqrt{2/3}d_{xz},$$
$$2e_y = \sqrt{1/3}d_{x^2-y^2} + \sqrt{2/3}d_{yz}. \quad (S1)$$

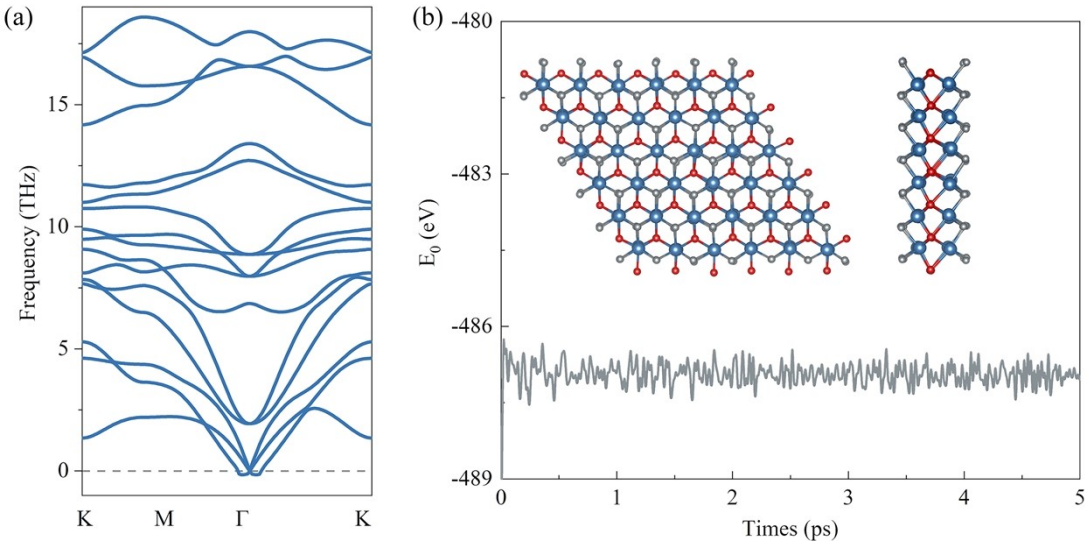

Fig. S1. (a) Phonon spectra and (b) AIMD simulation results of Co_2NF_2. Insert in (b) is snapshot of the structure for Co_2NF_2 taken from the end of AIMD simulations (500 K and 5 ps).

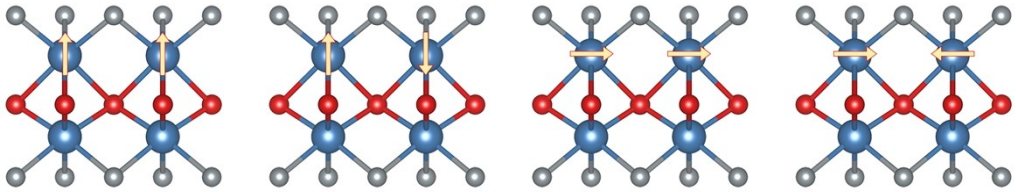

Fig. S2. Four different magnetic configurations used to obtain the magnetic parameters of J, λ and K_C.

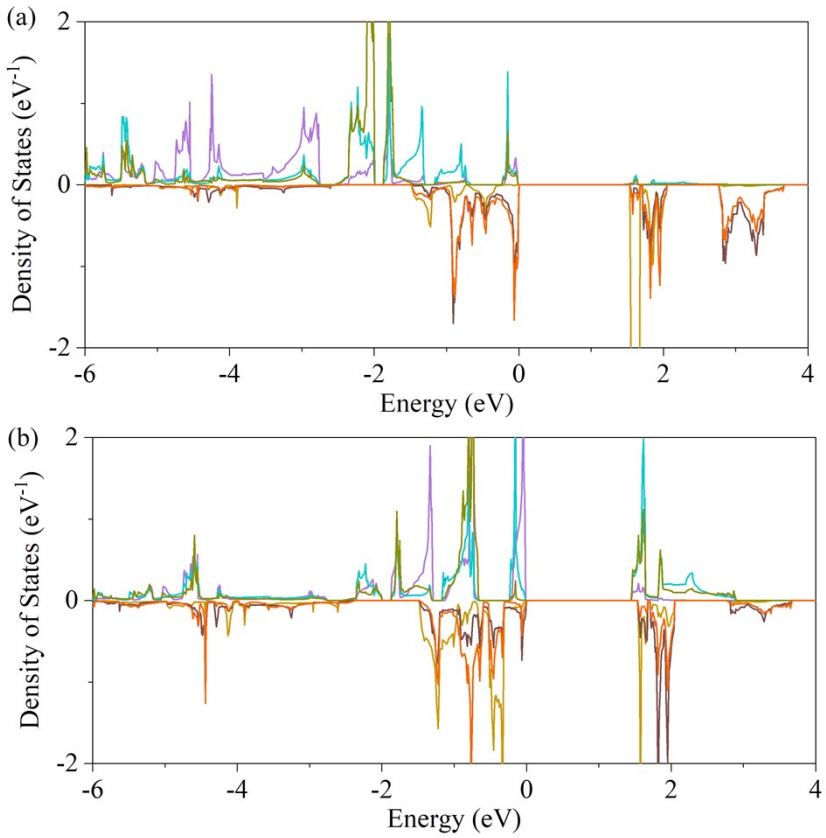

Fig. S3. PDOS for *d* orbitals of (a) Co1 atom and (b) Co2 atom in Co_2NF_2,

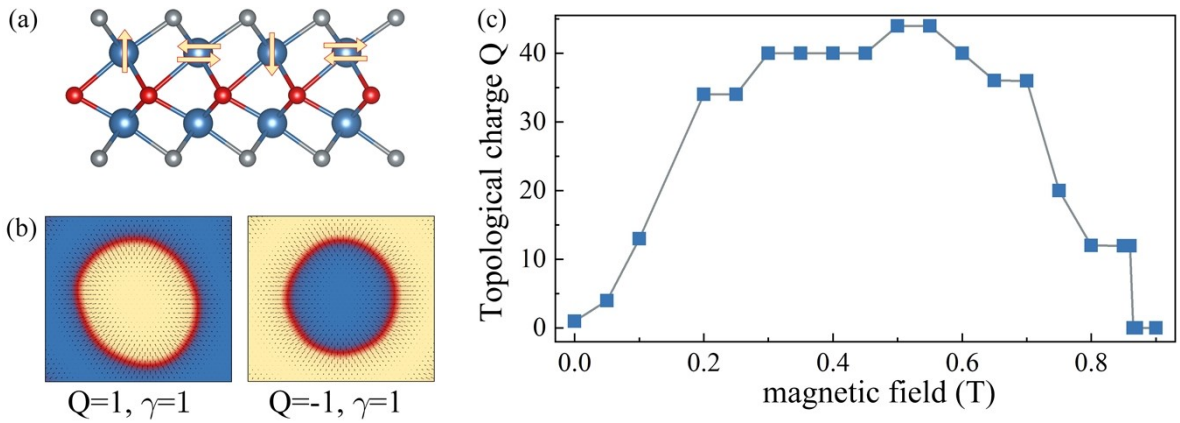

Fig. S4. (a) Two spin-spiral configurations of CW and ACW employed to obtain $d_{\parallel}$. (b) Zero-field magnetic skyrmions of Co_2NF_2. The color map specifies the OP spin component and arrows indicate the IP component. (c) Topological charge Q in Co_2NF_2 as a function of magnetic field.

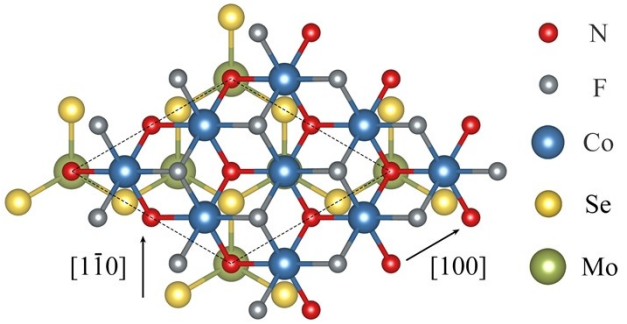

Fig. S5. Crystal structure of $Co_2NF_2/MoSe_2$ from top view, with dashed diamond indicating the unit cell.

Supplementary Note 3: The underlying physical mechanism for the variation of K_C between Co_2NF_2 and $Co_2NF_2/MoSe_2$.

K_C is substantially weakened for FE phases of $Co_2NF_2/MoSe_2$. To reveal the source of this character, we investigate the underlying physics for the single ion anisotropy K_C. It's well known that the single ion anisotropy originates from the joint effect of crystal field splitting and SOC. Through SOC effect, the isotropy spin angular momentum is coupled with the anisotropy orbital angular momentum induced by crystal field splitting, leading to K_C. According to the perturbation theory of SOC effect, K_C can be estimated as follows [10]:

$$K_C = \xi^2 \sum_{M,\, o,u,\sigma',\sigma} \sigma'\sigma \frac{\left|\langle u,\sigma|\hat{L}_z^{Co}|o,\sigma'\rangle\right|^2 - \left|\langle u,\sigma|\hat{L}_x^{Co}|o,\sigma'\rangle\right|^2}{E_{u,\sigma} - E_{o,\sigma'}}, (S2)$$

where u and o correspond to the unoccupied and occupied states of magnetic Co atoms near the Fermi level, respectively. $E_{u/o,\sigma}$ is the band energy of the state, and the spin indices σ/σ'=±1, referring to the two orthogonal spin states. The negative (positive) value of the K_C indicates OP (IP) single ion anisotropy.

In free-standing Co_2NF_2, as shown in **Fig. S3(a)**, $1a\downarrow$ is dominated in unoccupied states of Co1 atom, while the occupied states of Co1 atom is composed of $1e_{x/y}\downarrow$, $2e_{x/y}\uparrow$ and $1e_{x/y}\uparrow$. According to **Eq. S1** and **S2**, ($1a\downarrow$, $1e_{x/y}\downarrow$) is negative, while ($1a\downarrow$, $2e_{x/y}\uparrow$) and ($1a\downarrow$, $1e_{x/y}\uparrow$) are positive. Here, (u, o) represents the contribution from the SOC effect of the unoccupied state u and occupied state o to K_C. Owing to the small energy splitting between $1e_{x/y}\downarrow$ and $2e_{x/y}\uparrow$, ($1a\downarrow$, $1e_{x/y}\downarrow$) and ($1a\downarrow$, $2e_{x/y}\uparrow$) cancel each other, leading to a weak combined effect on K_C. Therefore, K_C is mainly contributed by ($1a\downarrow$, $1e_{x/y}\uparrow$), which is positive and consists with the OP magnetic anisotropy in Co_2NF_2. In $Co_2NF_2/MoSe_2$, as shown in **Fig. S6**, the energy splitting between $1e_{x/y}\downarrow$ and $2e_{x/y}\uparrow$ becomes larger as compared with that in Co_2NF_2. Thus, the negative ($1a\downarrow$, $1e_{x/y}\downarrow$) makes a greater contribution, indicating the substantially weakened K_C in $Co_2NF_2/MoSe_2$.

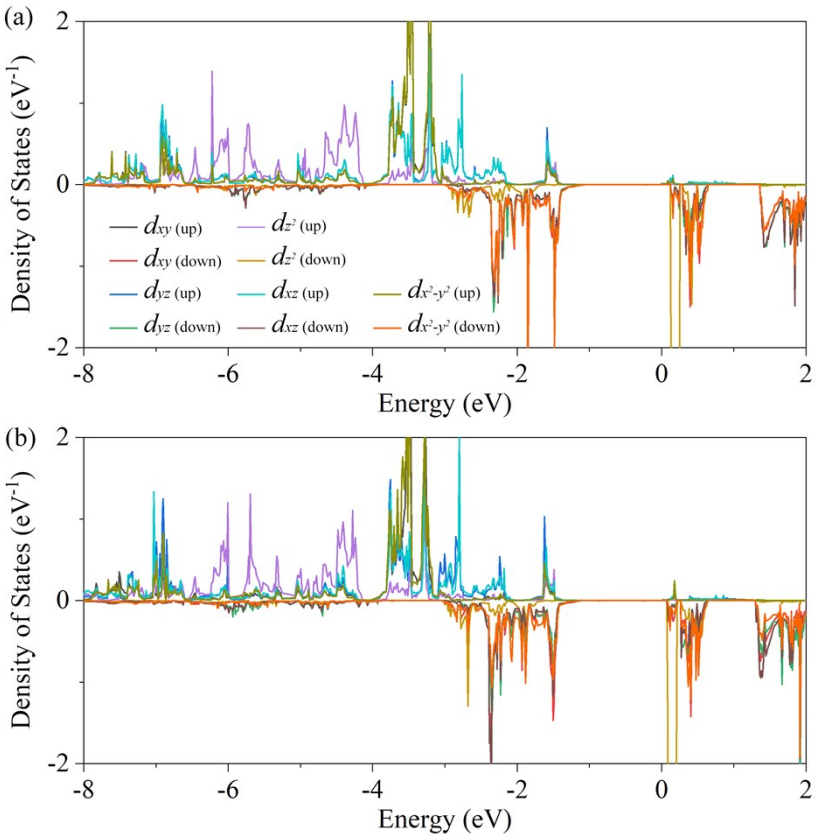

Fig. S6. PDOS for *d* orbitals of magnetic Co atom in (a) +P↑ state and (b) -P↓ state of $Co_2NF_2/MoSe_2$.

[1] Blöchl, P. E. Projector augmented-wave method. Phys. Rev. B 50, 17953 (1994).

[2] Kresse, G. and Hafner, J. Ab initio molecular-dynamics simulation of the liquid-metal–amorphous-semiconductor transition in germanium. Phys. Rev. B 49, 14251 (1994).

[3] Kresse, G. and Furthmüller, J. Efficient iterative schemes for ab initio total-energy calculations using a plane-wave basis set. Phys. Rev. B 54, 11169 (1996).

[4] Perdew, J. P., Burke, K. and Ernzerhof, M. Generalized gradient approximation made simple. Phys. Rev. Lett. 77, 3865 (1996).

[5] Rohrbach, A., Hafner, J. and Kresse, G. Electronic correlation effects in transition-metal sulfides. J. Phys.: Condens. Matter. 15, 979 (2003).

[6] Huang, C., Zhou, J., Sun, H., Wu, F., Hou, Y. and Kan, E., Toward Room-Temperature Electrical Control of Magnetic Order in Multiferroic van der Waals Materials. Nano Lett. 22, 5191 (2022).

[7] Grimme, S., Ehrlich, S. and Goerigk, L., Effect of the damping function in dispersion corrected density functional theory. J. Comput. Chem. 32, 1456 (2011).

[8] Neugebauer, J. and Scheffler, M., Adsorbate-substrate and adsorbate-adsorbate interactions of Na and K adlayers on Al (111). Phys. Rev. B 46, 16067 (1992).

[9] Miyatake, Y., Yamamoto, M., Kim, J. J., Toyonaga, M. and Nagai, O., On the implementation of the 'heat bath' algorithms for Monte Carlo simulations of classical Heisenberg spin systems. J. Phys. C: Solid State Phys. 19, 2539 (1986).

[10] Kim, J., Kim, K. W., Kim, B., Kang, C. J., Shin, D., Lee, S. H., Min, B. C. and Park, N., Exploitable magnetic anisotropy of the two-dimensional magnet CrI_3. Nano Lett. 20, 929 (2020).